Alternate protein kinase A activity identifies a unique population of stromal cells in adult bone

Kit Man Tsang[a,b], Matthew F. Starost[c], Maria Nesterova[a], Sosipatros A. Boikos[a], Tonya Watkins[d], Madson Q. Almeida[a], Michelle Harran[a], Andrew Li[a], Michael T. Collins[e], Christopher Cheadle[d], Edward L. Mertz[f], Sergey Leikin[f], Lawrence S. Kirschner[g], Pamela Robey[e], and Constantine A. Stratakis[a,h,1]

[a]Section on Endocrinology and Genetics, Program on Developmental Endocrinology and Genetics and [h]Pediatric Endocrinology Inter-institute Training Program, *Eunice Kennedy Shriver* National Institute of Child Health and Human Development, National Institutes of Health, Bethesda, MD 20892; [b]Division of Biochemistry (Medicine), School of Biomedical Sciences, Chinese University of Hong Kong, Hong Kong, China 00852; [c]Office of Research Services, Division of Veterinary Resources, National Institutes of Health, Bethesda, MD 20892; [d]Genomics Core, Division of Allergy and Clinical Immunology, Johns Hopkins University School of Medicine, Baltimore, MD 21224; [e]Craniofacial and Skeletal Diseases Branch, National Institute of Dental and Craniofacial Research, National Institutes of Health, Bethesda, MD 20892; [f]Section on Physical Biochemistry, Office of the Scientific Director, National Institute of Child Health and Human Development, National Institutes of Health, Bethesda, MD 20892; and [g]Department of Molecular Virology, Immunology and Molecular Genetics, Ohio State University, Columbus, OH 43210

Communicated by John B. Robbins, National Institutes of Health, Bethesda, MD, March 21, 2010 (received for review March 3, 2010)

A population of stromal cells that retains osteogenic capacity in adult bone (adult bone stromal cells or aBSCs) exists and is under intense investigation. Mice heterozygous for a null allele of *prkar1a* (*Prkar1a*$^{+/-}$), the primary receptor for cyclic adenosine monophosphate (cAMP) and regulator of protein kinase A (PKA) activity, developed bone lesions that were derived from cAMP-responsive osteogenic cells and resembled fibrous dysplasia (FD). *Prkar1a*$^{+/-}$ mice were crossed with mice that were heterozygous for catalytic subunit Cα (*Prkaca*$^{+/-}$), the main PKA activity-mediating molecule, to generate a mouse model with double heterozygosity for *prkar1a* and *prkaca* (*Prkar1a*$^{+/-}$*Prkaca*$^{+/-}$). Unexpectedly, *Prkar1a*$^{+/-}$*Prkaca*$^{+/-}$ mice developed a greater number of osseous lesions starting at 3 months of age that varied from the rare chondromas in the long bones and the ubiquitous osteochondrodysplasia of vertebral bodies to the occasional sarcoma in older animals. Cells from these lesions originated from an area proximal to the growth plate, expressed osteogenic cell markers, and showed higher PKA activity that was mostly type II (PKA-II) mediated by an alternate pattern of catalytic subunit expression. Gene expression profiling confirmed a preosteoblastic nature for these cells but also showed a signature that was indicative of mesenchymal-to-epithelial transition and increased *Wnt* signaling. These studies show that a specific subpopulation of aBSCs can be stimulated in adult bone by alternate PKA and catalytic subunit activity; abnormal proliferation of these cells leads to skeletal lesions that have similarities to human FD and bone tumors.

catalytic subunit | mesenchymal cells | regulatory subunit | tumor | sarcoma

Genes *Prkar1a* and *prkaca* encode the type 1A regulatory subunit (R1α) and type A catalytic subunit (Cα), respectively, of cAMP (cAMP)-dependent protein kinase (PKA) (1). PKA exists as a holoenzyme that consists of a homodimer of regulatory subunits and two inactive catalytic subunits, each bound to one of the regulatory subunits of the dimer (2). Four main regulatory subunit isoforms (R1α, R1β, RIIα, and RIIβ) and four catalytic subunit isoforms (Cα, Cβ, Cγ, and Prkx) have been identified (2, 3). The holoenzyme of two molecules of catalytic subunits with dimers of R1α or R1β forms the PKA type I isozyme (PKA-I), whereas the complex with either RIIα or RIIβ forms the PKA type II isozyme (PKA-II) (2–4). PKA-I and -II have different cellular localizations, functions, and affinity to cAMP (3, 4).

Our previous studies have shown that *prkar1a* heterozygous mice (*Prkar1a*$^{+/-}$) develop various tumors, which include schwannomas, thyroid neoplasias, and tail bone lesions, in a spectrum that overlaps with that observed in Carney complex (CNC) patients (5). R1α haploinsufficiency leads to increased total PKA activity in response to cAMP and an increased PKA-II to PKA-I ratio (6–10). Dysregulation of the catalytic subunits appears to be the most important mechanism for an increase in cAMP-responsive PKA activity (11). Previous studies in mice and human cell lines have all suggested that coordinated inhibition of the catalytic subunit is the most important function of the PKA regulatory subunits (12–15). Accordingly, we hypothesized that if we studied the *Prkar1a*$^{+/-}$ animal in the background of *prkaca* haploinsufficiency (*Prkaca*$^{+/-}$), we would abrogate most if not all of the tumors that developed in the former (4, 6, 11, 15). However, the *Prkar1a*$^{+/-}$*Prkaca*$^{+/-}$ mice not only continued to develop bone lesions but also demonstrated a significant increase in both the number and the severity of the lesions, as well as a reduction in the age of first appearance of any bone abnormality. Biochemical characterization showed an overall increase in PKA activity, and protein expression studies showed an increase in type-II regulatory subunits and alternate PKA catalytic subunits in *Prkar1a*$^{+/-}$*Prkaca*$^{+/-}$ bone lesions. Histological analysis of bone from *Prkar1a*$^{+/-}$*Prkaca*$^{+/-}$ mice showed that these lesions had similarity to tumors from humans with CNC (16) (*SI Appendix*, Fig. S1) and some resemblance (but also differences) to humans and mice with fibrous dysplasia (FD), a disease of bone stromal cells (BSCs) (17, 18). Thus, genetic manipulation of the PKA pathway in mice revealed a particular population of BSCs in adult animals (aBSCs) that are responsive to cAMP signaling mediated mainly by PKA-II and alternate catalytic subunits. These data have implications for the understanding of bone marrow subgroups of cells and their potential pharmacological manipulation through the cAMP signaling pathway.

Results

Description and Evolution of Bone Lesions in *Prkar1a*$^{+/-}$*Prkaca*$^{+/-}$ Double Heterozygous Mice. None of the *Prkar1a*$^{+/-}$*Prkaca*$^{+/-}$ mice showed schwannomas or thyroid tumors that were found, as previously reported (5), in the *Prkar1a*$^{+/-}$ mice. However, we observed an increasing number of bone lesions along the tail of *Prkar1a*$^{+/-}$*Prkaca*$^{+/-}$ mice (Fig. 1*A*). A single male, 3 month-old *Prkar1a*$^{+/-}$*Prkaca*$^{+/-}$ mouse developed a tibial chondroma (*SI Appendix*, Fig. S2), a tumor analogous to what is seen in CNC patients (16). Tail lesions in *Prkar1a*$^{+/-}$*Prkaca*$^{+/-}$ mice first appeared at 4–5 months of age; 90% of *Prkar1a*$^{+/-}$*Prkaca*$^{+/-}$ mice

Author contributions: C.A.S. designed research; K.M.T., M.F.S., M.N., S.A.B., T.W., M.Q.A., M.H., A.L., M.T.C., E.L.M., S.L., and L.S.K. performed research; C.C. and S.L. contributed new reagents/analytic tools; K.M.T., M.F.S., M.N., M.T.C., P.R., and C.A.S. analyzed data; and K.M.T. and C.A.S. wrote the paper.

The authors declare no conflict of interest.

Data deposition: The raw and normalized microarray data reported in this paper have been deposited in the Gene Expression Omnibus (GEO) database, www.ncbi.nlm.nih.gov/geo (accession no. GSE20984).

[1]To whom correspondence should be addressed. E-mail: stratakc@cc1.nichd.nih.gov.

This article contains supporting information online at www.pnas.org/lookup/suppl/doi:10.1073/pnas.1003680107/-/DCSupplemental.

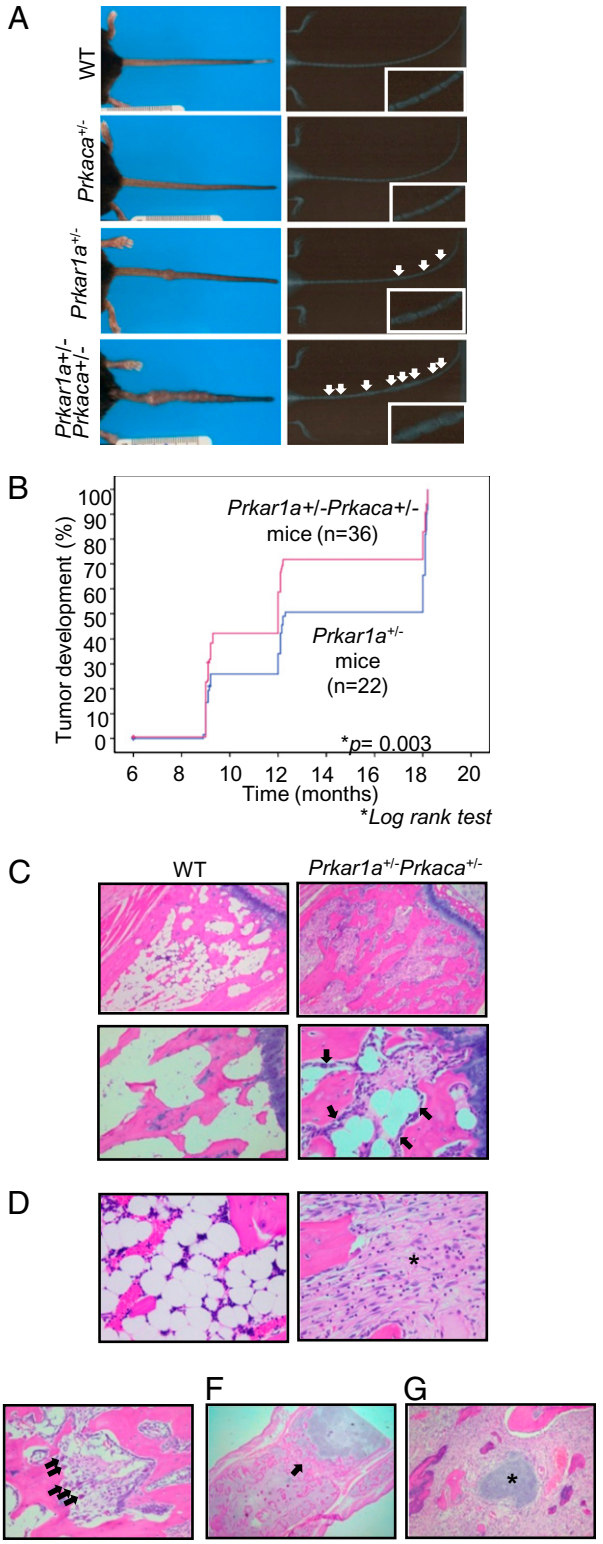

Fig. 1. Development of bone lesions along the tail of *Prkar1a*$^{+/-}$ and *Prkar1a*$^{+/-}$*Prkaca*$^{+/-}$ mice. (*A Left*) comparison of tails from WT, *Prkaca*$^{+/-}$, *Prkar1a*$^{+/-}$, and *Prkar1a*$^{+/-}$*Prkaca*$^{+/-}$ mice at 12 months old. (*A Right*) X-ray radiographs. White arrows point to the lesions. (*B*) Kaplan–Meier curve shows the number of tail masses found in various ages of *Prkar1a*$^{+/-}$ and *Prkar1a*$^{+/-}$*Prkaca*$^{+/-}$ mice. (*C–G*) Hematoxylin and eosin (H&E) staining of longitudinal sections of WT bones and *Prkar1a*$^{+/-}$*Prkaca*$^{+/-}$ bone lesions. In *C*, black arrows denote the presence of mature osteoblasts lining along the trabecular bone. (Original magnification: *C Upper*, ×10; *Lower*, original magnification, ×20 . In *D*, the asterisk denotes the bone marrow space filled with fibroblastoid cells. (Original magnification, ×40). In *E*, black arrows denote the presence of osteoclasts. (Original magnification: ×20.) In *F*, the black arrow denotes the destroyed joint space. (Original magnification: ×2.) In *G*, the asterisk denotes the presence of cartilage island within the fibroblasts. (Original magnification: ×20.)

exhibited these lesions by 6 months, and 100% by 9 months. *Prkar1a*$^{+/-}$*Prkaca*$^{+/-}$ mice not only developed these lesions earlier but also showed an increased number of lesions when compared to the age-matched *Prkar1a*$^{+/-}$ mice (Fig. 1*B*). Four of 30 *Prkar1a*$^{+/-}$ *Prkaca*$^{+/-}$ mice (13%) developed osteochondromyxoma (OCM), a tumor that was histologically similar to the bony lesions that have been reported in association with CNC (16). Cartilaginous metaplasia, chondromas, and osteochondrodysplasia were observed in marrow cavities of up to 1/3 of the long bones and in most of the vertebral bodies (up to 23% of the spinal column and 100% of the caudal vertebrae) of the *Prkar1a*$^{+/-}$*Prkaca*$^{+/-}$ mice. Two metastatic osteochondrosarcomas developed in one *Prkar1a*$^{+/-}$ mouse that was 16 months old and one *Prkar1a*$^{+/-}$*Prkaca*$^{+/-}$ mouse that was 14 months old; in both cases the most likely primary sites were hind-limb masses, and metastases were renal and lung, respectively (*SI Appendix*, Fig. S3).

Osteoblast-like cells lined along the trabecular bone in younger *Prkar1a*$^{+/-}$*Prkaca*$^{+/-}$ mice, and then gradually, with advancing age, filled the marrow with loosely arranged collagenous connective tissue and fibroblastoid cells (Fig. 1 *C* and *D*). As the marrow spaces were being filled, some of the trabeculae were being digested by activated osteoclasts (Fig. 1*E*). At about 12 months of age, all caudal vertebrae were affected in various degrees. As the new bone formation continued, it effaced the cartilaginous growth plate and eventually coalesced with adjacent masses encasing the joint space (Fig. 1*F*). With time, in some lesions, hyaline cartilage could fill up the marrow (Fig. 1*G*). These changes are presented in more detail and with more photographs in *SI Appendix*, *Results* and Fig. S4. The lesions always started from the area immediately under the growth plate and adjacent periosteal bone (*SI Appendix*, Fig. S5 and Fig. S6*A*). Successive vertebrae were affected in the *Prkar1a*$^{+/-}$*Prkaca*$^{+/-}$ mice, whereas this was unusual in *Prkar1a*$^{+/-}$ mice; the affected vertebrae were macroscopically visible by 9–12 months in all *Prkar1a*$^{+/-}$*Prkaca*$^{+/-}$ mice (*SI Appendix*, Fig. S5*B* and Fig. S6*B*). The periosteum of affected bones was also abnormal. First, occasionally, cells from lesions from *Prkar1a*$^{+/-}$ *Prkaca*$^{+/-}$ mice invaded and crossed the periosteum into the extraosseous space (*SI Appendix*, Fig. S7 *A* and *B*). Second, *Sharpey* fibers, characteristic of FD lesions (19), were present at various sites along the affected periosteum (*SI Appendix*, Fig. S7*C*). An increased number of apoptotic bodies within the rapidly proliferating cells was evident (*SI Appendix*, Fig. S7*D*), and osteocytes were morphologically abnormal within the newly formed osteoid (arrows in *SI Appendix*, Fig. S7 *B–D*).

Microcomputed Tomography (μCT) and Raman Microspectroscopy (RMS). μCT analysis of caudal vertebrae (Fig. 2*A*) revealed that the overall bone mineralization density of *Prkar1a*$^{+/-}$ and *Prkar1a*$^{+/-}$*Prkaca*$^{+/-}$ was significantly lower when compared to WT (Fig. 2*B*). A previously undocumented observation was that the single heterozygote, *Prkaca*$^{+/-}$ mice showed an overall gain in bone formation that was derived from primarily cortical bone; trabecular bone in *Prkaca*$^{+/-}$ mice tended to be decreased. In 6-month-old *Prkar1a*$^{+/-}$*Prkaca*$^{+/-}$ animals, brightfield and polarization transmission microscopy and RMS showed that in affected bones, normal cortical bone was replaced by mineralized material that had intermediate organization and mineralization heterogeneity closer to woven than to lamellar bone; the normally sharp mineralization boundary between periosteum and cortical bone was now replaced by a gradual increase of mineralization from the

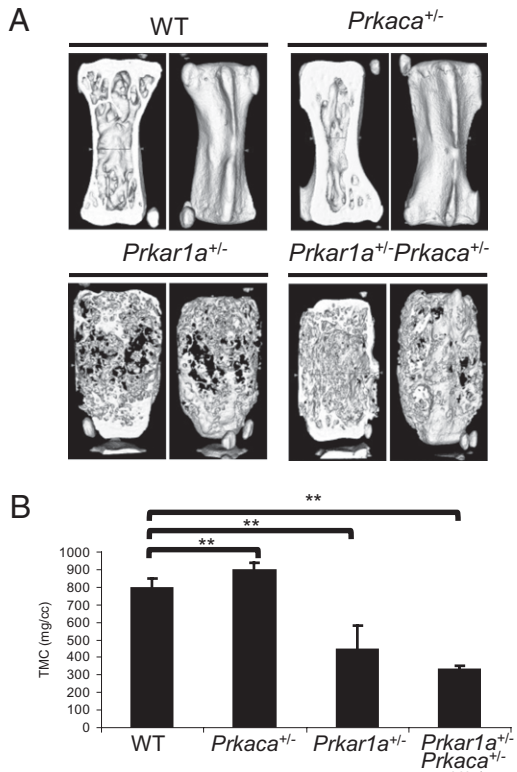

Fig. 2. Undermineralization of bone in both *Prkar1a*$^{+/-}$ and *Prkar1a*$^{+/-}$ *Prkaca*$^{+/-}$ mice. (*A*) μCT images of caudal vertebra from WT, *Prkaca*$^{+/-}$, *Prkar1a*$^{+/-}$, and *Prkar1a*$^{+/-}$*Prkaca*$^{+/-}$ mice at the age of 12 months. (*B*) Average of tissue mineral content (TMC) measurement of three caudal vertebrae from WT, *Prkaca*$^{+/-}$, *Prkar1a*$^{+/-}$, and *Prkar1a*$^{+/-}$*Prkaca*$^{+/-}$ mice at 12 months old. **, $P < 0.01$. Error bars represent means ± SD.

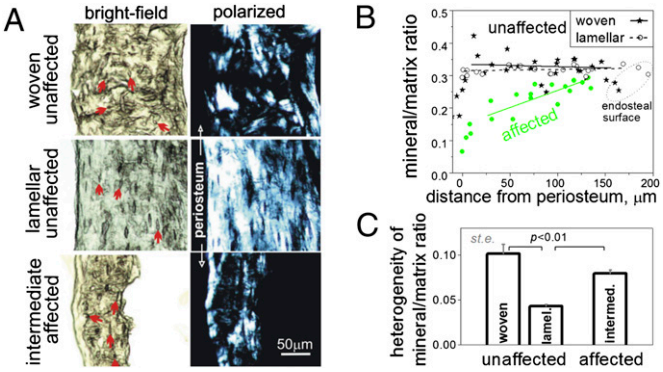

Fig. 3. Structure and mineralization of cortical bone in adjacent affected and unaffected caudal vertebrae. (*A*) Brightfield and polarized images of unaffected and affected caudal vertebrae. Well organized, lamellar/fine-fibered bone was indicated by well oriented spindle-shaped osteocyte lacunae (arrows) and more uniform polarized images due to regular collagen fiber orientation. Woven bone was indicated by irregular-shaped, disoriented lacunae and patchy appearance of polarized images due to irregular fiber orientation. (*B*) Even (−0.1 ± 0.2 mm^{-1} slope) mineral/matrix ratio across the cortical layer (the intensity ratio of mineral PO_4 to organic CH Raman peaks) is characteristic of well mineralized, mature bone in unaffected vertebrae. Gradually increasing mineral/matrix ratio from periosteal to endosteal surface [+0.8 ± 0.2 (SD) mm^{-1} slope, $P < 0.003$] indicates lagging mineralization characteristic of rapidly growing, immature bone in affected vertebrae. (*C*) High mineralization heterogeneity (coefficient of variation for the mineral/matrix ratio) in all cortical regions of affected vertebrae is also consistent with rapid formation of immature bone.

periosteal to the endosteal surface (Fig. 3), indicating a lag between bone matrix formation and mineralization and abnormal coordination of these processes with bone resorption.

Characterization of Cells Forming the Lesions in Affected Bones. We compared gene expression between *Prkar1a*$^{+/-}$ and *Prkar1a*$^{+/-}$ *Prkaca*$^{+/-}$ bone lesions (*SI Appendix*, Table S1) and *Runx2*, the master regulator of osteogenic commitment (20), was significantly up-regulated in the latter at both the mRNA and protein level (*SI Appendix*, Fig. S8). On the other hand, the fibroblast-like cells did not show a strong signal for osteocalcin, a marker of mature osteoblasts (*SI Appendix*, Fig. S9*A*), and were negative for osteopontin, as in *Prkar1a*$^{+/-}$ mice (5); the only cells in the lesions that stained for osteocalcin were those that lined the trabeculae (*SI Appendix*, Fig. S9*A*). Taken together, these data suggested that the fibroblastoid cells within the lesions were committed osteogenic (*Runx-2*-positive), unlike the case in *Prkar1a*$^{+/-}$ lesions (5). Furthermore, cells lining newly formed bone were more mature osteoblasts. Osteoclasts were also activated in the lesions: tartrate-resistant acid phosphatase 5 (Acp5) and cathepsin K were highly expressed in the cells lined along the trabeculae bone as well as inside the pool of fibrotic cells of bone lesions from *Prkar1a*$^{+/-}$ *Prkaca*$^{+/-}$; only the cells next to the trabecular bone expressed these markers in *Prkar1a*$^{+/-}$ lesions (*SI Appendix*, Fig. S9*B*).

PKA and Phosphodiesterase (PDE) Activities. The loss of one *prkar1a* allele and one *prkaca* allele led to an increase in cAMP-stimulated kinase activity in bone tumors (*Prkar1a*$^{+/-}$*Prkaca*$^{+/-}$ tumor vs. WT tail bone, 2,724.7 ± 866.8 vs. 912.4 ± 283.6, $P < 0.05$). *Prkar1a*$^{+/-}$ tumors had a smaller increase in kinase activity when compared to WT bone ($P = 0.079$) (*SI Appendix*, Fig. S10*A*), consistent with previously published data (5). Like in *Prkar1a*$^{+/-}$ tumors (5), the bone lesions from *Prkar1a*$^{+/-}$*Prkaca*$^{+/-}$ mice did not show any loss of heterozygosity (LOH) of the normal *Prkar1a* or *Prkaca* allele (*SI Appendix*, Fig. S11). cAMP levels were slightly increased in bone tumors from both *Prkar1a*$^{+/-}$ and *Prkar1a*$^{+/-}$*Prkaca*$^{+/-}$ mice (*SI Appendix*, Fig. S10*B*). To address whether this increase in cAMP levels was the result of a decrease in PDE activity, we measured the latter. Total PDE activity in tumor protein extracts was significantly increased in both *Prkar1a*$^{+/-}$- and *Prkar1a*$^{+/-}$*Prkaca*$^{+/-}$-induced tumors (*SI Appendix*, Fig. S10*C*). By Western blot analysis, we determined that cAMP-binding Pde11a and Pde4d, but not Pde7a, were highly expressed in tumor cells (*SI Appendix*, Fig. S10*D*). Therefore, the increase in cAMP levels did not result from a decrease in total PDE activity. We then looked at the expression of adenylate cyclases (AC, *Adcy*) in the bone lesions. We tested all nine transmembrane AC enzymes and the one soluble AC; *Adcy1*, *Adcy6*, and *Adcy9* were found to be up-regulated at both the mRNA and protein level (*SI Appendix*, Fig. S12). Thus, the increase in cAMP levels was at least in part mediated by an increased expression of ACs.

PKA Typing, Regulatory, and Catalytic Subunits. We then performed diethylaminoethyl cellulose (DEAE) ion-exchange column chromatography on total proteins extracted from the primary cells derived from bone tumors and normal bone tissues (Fig. 4). *Prkar1a*$^{+/-}$ *Prkaca*$^{+/-}$ tumor cells had significantly more PKA-II complexes (PKA-II to PKA-I ratio = 3.10, $P = 0.057$ compared to WT; $P < 0.001$ compared to *Prkar1a*$^{+/-}$) (Fig. 4*A Lower Right*). These data indicated that there was an excess of PKA-II in the lesions. Consistent with these data, Western blot analysis showed an up-regulated expression of type II regulatory subunits in bone tumors (Fig. 4*B*), also confirmed by IHC (*SI Appendix*, Fig. S13). By using an antibody specific for the phosphorylated form, we showed an increase in phosphorylated forms of type II regulatory subunits in the tumors from *Prkar1a*$^{+/-}$*Prkaca*$^{+/-}$ mice (Fig. 4*B*). Both *Prkar1a*$^{+/-}$- and *Prkar1a*$^{+/-}$*Prkaca*$^{+/-}$-derived tumor showed an induction in the expression of Prkx and Cβ1 and a reduction in Cβ2 when compared with WT bone tissue. When tumors from *Prkar1a*$^{+/-}$ mice were compared to those of *Prkar1a*$^{+/-}$*Prkaca*$^{+/-}$

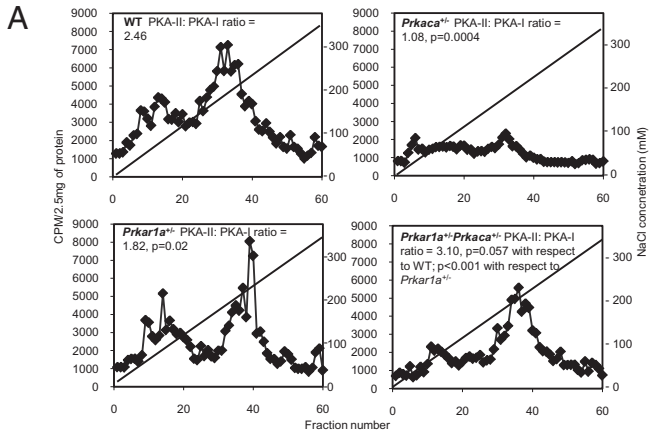

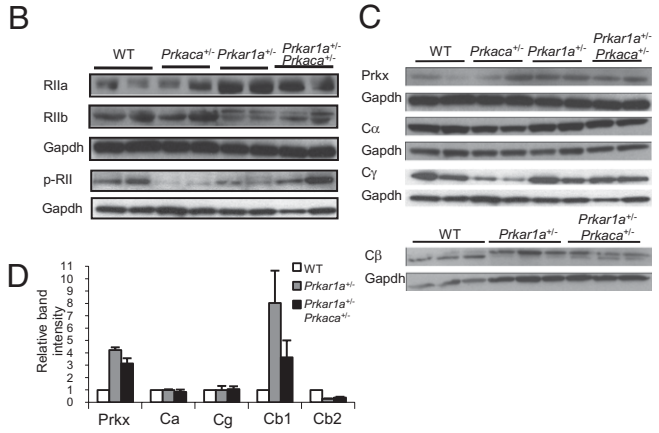

Fig. 4. Increased PKA-II complex, type II regulatory subunit and catalytic subunit β1, and Prkx in *Prkar1a*$^{+/-}$*Prkaca*$^{+/-}$ mice bone tumors. (*A*) DEAE-chromatography of PKA isozymes in tail tissues of WT and *Prkaca*$^{+/-}$ mice and tail lesions of *Prkar1a*$^{+/-}$ and *Prkar1a*$^{+/-}$*Prkaca*$^{+/-}$ mice. PKA-II to PKA-I ratio was calculated from averaging the intensities of 10 fractions within the peaks. Note that tail lesions of *Prkar1a*$^{+/-}$*Prkaca*$^{+/-}$ mice had the highest PKA-II to PKA-I ratio (n = 3). (*B*) Western blot analysis on RIIα, RIIβ, and phosphorylated form of RII in WT, *Prkaca*$^{+/-}$, *Prkar1a*$^{+/-}$, and *Prkar1a*$^{+/-}$*Prkaca*$^{+/-}$ mice at 1 year of age, showing the up-regulation of RII subunits in bone lesions and increase in phosphorylated form of RII in *Prkar1a*$^{+/-}$*Prkaca*$^{+/-}$ tumors. (*C*) Western blot analysis on different PKA catalytic subunits of WT, *Prkaca*$^{+/-}$, *Prkar1a*$^{+/-}$, and *Prkar1a*$^{+/-}$*Prkaca*$^{+/-}$ mice at 1 year of age. (*D*) Relative quantification of Prkx, Cα, Cγ, Cβ1, and Cβ2 protein in bone lesions against WT normal bone.

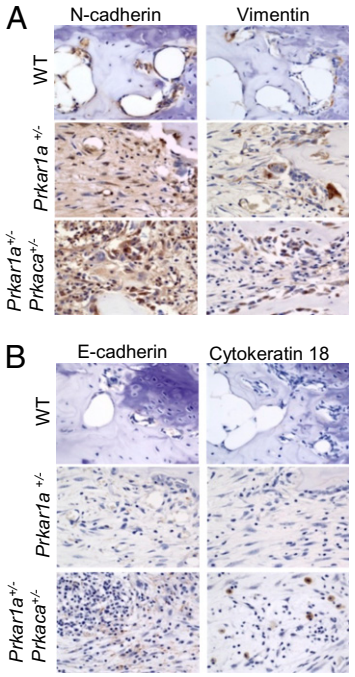

Fig. 5. Expression of mesenchymal proteins in bone lesions from *Prkar1a*$^{+/-}$ and *Prkar1a*$^{+/-}$*Prkaca*$^{+/-}$ mice and epithelial markers in *Prkar1a*$^{+/-}$*Prkaca*$^{+/-}$ bone tumors that confirms the mesenchymal-to-epithelial gene signature in lesions from *Prkar1a*$^{+/-}$*Prkaca*$^{+/-}$ mice. (*A*) Immunohistochemistry for n-cadherin and vimentin, mesenchymal proteins, is increased in all animals of PKA defects. (*B*) Immunohistochemistry for e-cadherin and cytokeratin 18, epithelial proteins, is increased in double heterozygote animals only.

animals, the latter had a higher expression of Cβ2 (Fig. 4 *C* and *D*). IHC confirmed that Cβ, Cγ, and the Prkx proteins, in addition to Cα, were up-regulated in the bone lesions (*SI Appendix*, Fig. S14).

Gene Signature of Bone Lesions. Tumor tissues from *Prkar1a*$^{+/-}$ and *Prkar1a*$^{+/-}$*Prkaca*$^{+/-}$ mice had similar whole-genome gene expression signatures when compared against WT tail bone (*SI Appendix*, Fig. S15*A*). Both expressed high levels of mesenchymal markers, like *n-cadherin*, *vimentin*, *snail1*, *twist*, *mmp2*, *mmp9*, *tgfb1*, and *col1a1* (*SI Appendix*, Table S1 and Table S2*A*); confirmed by IHC studies, mesenchymal proteins n-cadherin and vimentin were highly expressed by abnormally proliferating fibroblasts in bone lesions (Fig. 5*A*). Western blot analysis also confirmed the induction of mmp2 and mmp9 protein expression in bone tumors (*SI Appendix*, Fig. S16*A*). We then compared *Prkar1a*$^{+/-}$ and *Prkar1a*$^{+/-}$*Prkaca*$^{+/-}$ bone tumors with a clustering algorithm (21) (*SI Appendix*, Fig. S15*B*). The raw and normalized array data have been deposited in National Center for Biotechnology Information's Gene Expression Omnibus (GEO) (22) and are accessible through GEO Series accession number GSE20984. We identified 258 significantly up-regulated genes in *Prkar1a*$^{+/-}$*Prkaca*$^{+/-}$-derived tumors; they included 20 genes associated with hair and epithelial differentiation, such as keratin and keratin-related genes, *S100A3*, *Bmp4*, *Msx1*, *Foxq1*, and *Foxn1* (*SI Appendix*, Table S2*B*). IHC staining for epithelial markers, E-cadherin and cytokeratin 18 (Fig. 5*B*), also revealed that, whereas most of the fibroblast-like cells were mesenchymal, islands of cells within the *Prkar1a*$^{+/-}$*Prkaca*$^{+/-}$ lesions expressed epithelial markers. Several other genes were increased in the *Prkar1a*$^{+/-}$*Prkaca*$^{+/-}$ tumors including *cFos* and *Foxo1*; IHC confirmed these data (*SI Appendix*, Fig. S16*B*). However, what appeared to be the most up-regulated molecular pathway in these lesions was that of the *Wnt* signaling. We then performed RT-qPCR array analysis of *Wnt* signaling pathway genes (n = 84) that showed that the lesions from *Prkar1a*$^{+/-}$*Prkaca*$^{+/-}$ mice had increased expression of *brachyury* (the *T* gene), *Wnt3*, *Wnt3a*, *Wnt7a*, *Wnt8a*, and *Wnt8b* (*SI Appendix*, Table S3). In accordance, the lesions also showed down-regulation of *Wnt* signaling pathway inhibitors, such as *Dkk1*. *Brachyury* was also increased by IHC in lesions from *Prkar1a*$^{+/-}$*Prkaca*$^{+/-}$ mice (*SI Appendix*, Fig. S16*B*). FACS studies on the primary cultures of bone tumors confirmed the mesenchymal nature of the cells because they expressed high level of vimentin, c-fos, c-kit, and foxo1 (*SI Appendix*, Fig. S17). Ninety percent of these cells also expressed CD44, CD90, and Vcam but stained negative for CD45 (*SI Appendix*, Fig. S18).

Discussion

The present study demonstrates that tissues are extraordinarily sensitive to modest changes in the type of PKA signaling (1, 2, 4). PKA abnormalities were enhanced in the bone of the *Prkar1a*$^{+/-}$*Prkaca*$^{+/-}$ mice by cAMP levels that were associated with increased expression of Adcy1, Adcy6, and Adcy9 (*SI Appendix*, Fig. S12), despite a concurrent increase in PDE activity. Low vs. high in-

tracellular cAMP levels have been known for years to have different effects on bone physiology (23), and cAMP signaling is essential for normal bone development (24) in response to parathyroid hormone (PTH) and PTH-related protein (PTHrP). Moreover, PKA is a powerful negative regulator of all *hedgehog* signaling, which ensures conversion of BSCs to chondrocytes and osteoblasts (24, 25) in vertebrates and in a variety of settings (26–28). PKA is activated by PTH or PTHrP through the G protein stimulating subunit (Gs_{α},) and activation of the Adcy-dependent generation of cAMP. Activation of Gs_{α} leads to FD in humans (18) and mice (17), a disease affecting BSCs (29). *Gnas* overexpression leads to primarily PKA-II activation (30) but does not lead to AC (*Adcy*) activation in vitro or in vivo (30, 31). On the other hand, decreased *GNAS* expression in human mesenchymal cells leads to a more mature-osteoblast-like phenotype and decreased PKA-II activity (32). These data converge in the following hypothesis: PKA activation either by PTHRP or Gs_{α} (17, 24, 30, 33, 34), through cAMP, or by deficient inhibitory control of the catalytic subunit Cα (1, 11) leads to excess PKA-II, recruitment of BSCs from the pool of bone marrow mesenchymal cells, and their differentiation to and proliferation as chondrocytes and immature osteoblasts. These cells are unable to follow the regular process of maturation to hypetrophic chondrocytes or mature osteoblasts and develop a matrix that is irregular and undermineralized (Fig. 3).

Are the bone lesions that we see in *Prkar1a*$^{+/-}$*Prkaca*$^{+/-}$ mice consistent with FD? Despite the similarities noted above, there are some important differences. First, the defects that we saw in *Prkar1a*$^{+/-}$*Prkaca*$^{+/-}$ mice developed postnatally, starting well after 2 months and peaking between 6 and 9 months of age. In human FD, lesions are present in toddlerhood and peak in late childhood and young adulthood (17, 18). Second, in both humans (18) and mice (17) with FD, the disease is caused by a postzygotic defect; all bones are chimeras of normal and abnormal Gs_{α}, which creates a totally different tissue microenvironment. In *Prkar1a*$^{+/-}$ and *Prkar1a*$^{+/-}$ *Prkaca*$^{+/-}$ mice, as well as humans with CNC, the defect is in the germline and the mutant allele is present in all cells (5, 16, 35). PKA defects appear to affect specific areas that are characterized by high amount of metabolically active trabecular bone and residual cartilage (such as adult mouse vertebrae) or have a high natural population of prechondrocytes (i.e., tibia). It is of note that the earliest lesion in *Prkar1a*$^{+/-}$*Prkaca*$^{+/-}$ mice was a tibial chondroma (*SI Appendix*, Fig. S2); in humans with CNC, humerus and tibia are the most frequently affected long bones, too (16). Thus, unlike in FD, PKA defects reveal a particular population of aBSCs. These cells obviously belong to the osteoblastic lineage and appear to originate in affected bones from an area under the growth plate of the long bones and the vertebrae.

The identified stromal cells expressed alkaline phosphatase (*Alp1*) (*SI Appendix*, Table S1), osteocalcin (*SI Appendix*, Fig. S9*A*), *cFos* (*SI Appendix*, Fig. S16*B*), as in FD (36), collagen I, matrix metalloproteinases (MMP) 9 and MMP10, and other known markers of bone development. There were some significant differences between *Prkar1a*$^{+/-}$ and *Prkar1a*$^{+/-}$*Prkaca*$^{+/-}$ cells. *Prkar1a*$^{+/-}$*Prkaca*$^{+/-}$ cells were closer to chondrocytes than osteocytes in their gene signature (*SI Appendix*, Table S1): they expressed less *Alp1* and bone morphogenetic protein-2 (*Bmp2*) but expressed more Collagen 11 (*Col11a1*), the gene mutated in the chondrodysplastic (*cho*) mouse (37), enamel, *Bmp4*, fibroblast growth factor receptor 2 (*Fgfr2*), and Smad 1. The latter molecules pointed to a gene signature of *Prkar1a*$^{+/-}$*Prkaca*$^{+/-}$ cells that is closer to that of cells involved in ectopic ossification in *fibrodysplasia ossificans progressiva* (FOP) (38): overexpression of BMP4 (39) and SMAD1 (40) is seen in human cells from this condition. Furthermore, proximal chondromas in the tibia, the long bone most affected in *Prkar1a*$^{+/-}$*Prkaca*$^{+/-}$ mice (*SI Appendix*, Fig. S2), in humans with CNC (16), and in a chondrocyte-specific knockout mouse model of *Gnas* by ectopic cartilage formation (41), occur in >90% of patients with FOP (42). It is thus conceivable that the aBSCs identified in the bone of *Prkar1a*$^{+/-}$*Prkaca*$^{+/-}$ mice are as pluripotential as those progenitor cells that contribute to ectopic bone formation after activation of inflammation in FOP (43). *Prkar1a*$^{+/-}$*Prkaca*$^{+/-}$ cells also showed, as in other settings of R1α defects (44, 45) in humans and mice, induction of *Wnt*-signaling genes (*SI Appendix*, Table S3), including β-catenin and *brachyury*, and had a molecular signature consistent with mesenchymal-to-epithelial transition (*SI Appendix*, Table S2), which has also been seen in complete R1α loss (46).

We conclude that genetic manipulation of the PKA pathway in mice revealed a particular population of aBSCs that are responsive to cAMP signaling mediated mainly by PKA-II and alternate PKA catalytic subunits. It has only been recently recognized that stromal or mesenchymal cells respond to cAMP in vitro (29, 47); it was also shown that BSCs need proximity to cartilage for growth, proliferation, and differentiation (48). Our study extends these observations in vivo. The discovery of an alternate PKA activity as a factor that develops aBSCs had not been recognized earlier. These data may help in growing these cells ex vivo and explain some of the inconsistencies noted by investigators on cAMP signaling and growth of mesenchymal cells (47, 49–51). The present data are also helpful in understanding better the process of malignant transformation for which BSCs and other pluripotential cells are at risk (52). Finally, our study provides a mouse model of an FD-like condition caused by a germline defect.

Materials and Methods

Details are provided in *SI Appendix*, *Materials and Methods*.

Generation of *Prkar1a*$^{+/-}$*Prkaca*$^{+/-}$ Double Heterozygous Mice. *Prkar1a* heterozygous mice (*Prkar1a*$^{+/-}$), which contain one null allele of *Prkar1a*$^{\Delta 2}$, were previously generated in our laboratory (5). *Prkaca* heterozygous mice (*Prkaca*$^{+/-}$), which have a neomycin resistance cassette to replace exons 6–8 of the *prkaca* gene (53), were purchased from Mutant Mouse Regional Resource Centers (MMRRC) (strain name: B6; 129 × 1-Prkaca^{tm1Gsm}/Mmnc).

X-Ray, μCT, and RMS. The macroscopic and microscopic structure of the lesions were analyzed by radiographs using a Faxitron x-ray system (Model MX-20). μCT analysis employed a GE Medical Systems eXplore Locus SP μCT scanner and RMS using confocal Raman microscope (Senterra; Bruker Optics).

Flow Cytometry. Primary cells from bone tumors (1×10^5) were collected from cultures and fixed using the Cytofix/Cytoperm Fixation/Permeabilization Solution Kit (BD Biosciences). Primary antibodies: vimentine, foxo1, c-fos, c-kit, runx2, collagen 1, CD44, CD45, CD90, and Vcam (*SI Appendix*, Table S4) were used for staining. FITC-tag secondary antibody (1:250) (Invitrogen) was used for detection. MC3T3 (ATCC CRL-2593), which is a preosteoblastic cell line, was used as control cells.

PKA, PDE Activity, and cAMP Assays. PKA enzymatic activity was measured by the method described in ref. 54. cAMP levels were determined with the ^{3}H Biotrak Assay System (Amersham Biosciences). PDE activity was assayed with [H^3]-cAMP (55).

DEAE-Cellulose Chromatography. This experiment was performed as described in ref. 56.

ACKNOWLEDGMENTS. We thank Dr. J. Aidan Carney (Mayo Clinic, Rochester, MN) for examples of human tumors associated with CNC; Dr. Nicholas Patronas (Department of Diagnostic Radiology, National Institutes of Health Clinical Center) for sharing the clinical imaging of bone lesions from CNC patients; Dr. Kenn Holmbeck and Dr. Joanne Shi (National Institute of Dental and Craniofacial Research) for technical expertise in μCT experiment; Drs. Jean-Charles Grivel (National Institute of Child Health and Human Development), Iusta Caminha (National Institute of Allergy and Infectious Diseases, Bethesda, MD), and Joao Bosco Oliveira (National Institute of Allergy and Infectious Diseases) for technical expertise in flow cytometry study; and Dr. Robert M. Kotin (National Heart, Lung, and Blood Institute, Bethesda, MD) for generously providing us with the Prkx antibody. This work was supported by National Institutes of Health, Eunice Kennedy Shriver National Institute of Child Health and Human Development Intramural Project Z01-HD-000642-04 (to C.A.S.).

1. Bossis I, Stratakis CA (2004) Minireview: PRKAR1A: normal and abnormal functions. *Endocrinology* 145:5452–5458.
2. Skalhegg BS, Tasken K (2000) Specificity in the cAMP/PKA signaling pathway. Differential expression,regulation, and subcellular localization of subunits of PKA. *Front Biosci* 5:D678–D693.
3. Gamm DM, Baude EJ, Uhler MD (1996) The major catalytic subunit isoforms of cAMP-dependent protein kinase have distinct biochemical properties in vitro and in vivo. *J Biol Chem* 271:15736–15742.
4. McKnight GS, et al. (1988) Analysis of the cAMP-dependent protein kinase system using molecular genetic approaches. *Recent Prog Horm Res* 44:307–335.
5. Kirschner LS, et al. (2005) A mouse model for the Carney complex tumor syndrome develops neoplasia in cyclic AMP-responsive tissues. *Cancer Res* 65:4506–4514.
6. Amieux PS, et al. (1997) Compensatory regulation of RIalpha protein levels in protein kinase A mutant mice. *J Biol Chem* 272:3993–3998.
7. Griffin KJ, et al. (2004) Down-regulation of regulatory subunit type 1A of protein kinase A leads to endocrine and other tumors. *Cancer Res* 64:8811–8815.
8. Griffin KJ, et al. (2004) A mouse model for Carney complex. *Endocr Res* 30:903–911.
9. Griffin KJ, et al. (2004) A transgenic mouse bearing an antisense construct of regulatory subunit type 1A of protein kinase A develops endocrine and other tumours: comparison with Carney complex and other PRKAR1A induced lesions. *J Med Genet* 41:923–931.
10. Robinson-White A, et al. (2006) PRKAR1A Mutations and protein kinase A interactions with other signaling pathways in the adrenal cortex. *J Clin Endocrinol Metab* 91:2380–2388.
11. Meoli E, et al. (2008) Protein kinase A effects of an expressed PRKAR1A mutation associated with aggressive tumors. *Cancer Res* 68:3133–3141.
12. Herberg FW, Doyle ML, Cox S, Taylor SS (1999) Dissection of the nucleotide and metal-phosphate binding sites in cAMP-dependent protein kinase. *Biochemistry* 38: 6352–6360.
13. Kim C, Xuong NH, Taylor SS (2005) Crystal structure of a complex between the catalytic and regulatory (RIalpha) subunits of PKA. *Science* 307:690–696.
14. Kirschner LS, et al. (2000) Genetic heterogeneity and spectrum of mutations of the PRKAR1A gene in patients with the carney complex. *Hum Mol Genet* 9: 3037–3046.
15. Taylor SS, et al. (2005) Dynamics of signaling by PKA. *Biochim Biophys Acta* 1754: 25–37.
16. Carney JA, et al. (2001) Osteochondromyxoma of bone: a congenital tumor associated with lentigines and other unusual disorders. *Am J Surg Pathol* 25:164–176.
17. Bianco P, et al. (1998) Reproduction of human fibrous dysplasia of bone in immunocompromised mice by transplanted mosaics of normal and Gsalpha-mutated skeletal progenitor cells. *J Clin Invest* 101:1737–1744.
18. Riminucci M, et al. (1999) The histopathology of fibrous dysplasia of bone in patients with activating mutations of the Gs alpha gene: site-specific patterns and recurrent histological hallmarks. *J Pathol* 187:249–258.
19. Kashima TG, et al. (2009) Periostin, a novel marker of intramembranous ossification, is expressed in fibrous dysplasia and in c-Fos-overexpressing bone lesions. *Hum Pathol* 40:226–237.
20. Ducy P, Zhang R, Geoffroy V, Ridall AL, Karsenty G (1997) Osf2/Cbfa1: a transcriptional activator of osteoblast differentiation. *Cell* 89:747–754.
21. Eisen MB, Spellman PT, Brown PO, Botstein D (1998) Cluster analysis and display of genome-wide expression patterns. *Proc Natl Acad Sci USA* 95:14863–14868.
22. Edgar R, Domrachev M, Lash AE (2002) Gene Expression Omnibus: NCBI gene expression and hybridization array data repository. *Nucleic Acids Res* 30:207–210.
23. Klein DC, Raisz LG (1971) Role of adenosine-3′,5′-monophosphate in the hormonal regulation of bone resorption: studies with cultured fetal bone. *Endocrinology* 89: 818–826.
24. Kronenberg HM (2003) Developmental regulation of the growth plate. *Nature* 423: 332–336.
25. Long F, Zhang XM, Karp S, Yang Y, McMahon AP (2001) Genetic manipulation of hedgehog signaling in the endochondral skeleton reveals a direct role in the regulation of chondrocyte proliferation. *Development* 128:5099–5108.
26. Amieux PS, et al. (2002) Increased basal cAMP-dependent protein kinase activity inhibits the formation of mesoderm-derived structures in the developing mouse embryo. *J Biol Chem* 277:27294–27304.
27. Hammerschmidt M, Bitgood MJ, McMahon AP (1996) Protein kinase A is a common negative regulator of Hedgehog signaling in the vertebrate embryo. *Genes Dev* 10: 647–658.
28. Jiang J, Struhl G (1995) Protein kinase A and hedgehog signaling in Drosophila limb development. *Cell* 80:563–572.
29. Riminucci M, Saggio I, Robey PG, Bianco P (2006) Fibrous dysplasia as a stem cell disease. *J Bone Miner Res* 21 (Suppl 2):125–131.
30. Huang XP, Song X, Wang HY, Malbon CC (2002) Targeted expression of activated Q227L G(alpha)(s) in vivo. *Am J Physiol Cell Physiol* 283:C386–C395.
31. Gaudin C, et al. (1995) Overexpression of Gs alpha protein in the hearts of transgenic mice. *J Clin Invest* 95:1676–1683.
32. Lietman SA, Ding C, Cooke DW, Levine MA (2005) Reduction in Gsalpha induces osteogenic differentiation in human mesenchymal stem cells. *Clin Orthop Relat Res* (434):231–238.
33. Bastepe M, et al. (2004) Stimulatory G protein directly regulates hypertrophic differentiation of growth plate cartilage in vivo. *Proc Natl Acad Sci USA* 101: 14794–14799.
34. Sakamoto A, et al. (2005) Deficiency of the G-protein alpha-subunit G(s)alpha in osteoblasts leads to differential effects on trabecular and cortical bone. *J Biol Chem* 280:21369–21375.
35. Pavel E, Nadella K, Towns WH, 2nd, Kirschner LS (2008) Mutation of Prkar1a causes osteoblast neoplasia driven by dysregulation of protein kinase A. *Mol Endocrinol* 22: 430–440.
36. Candeliere GA, Glorieux FH, Prud'homme J, St-Arnaud R (1995) Increased expression of the c-fos proto-oncogene in bone from patients with fibrous dysplasia. *N Engl J Med* 332:1546–1551.
37. Li Y, et al. (1995) A fibrillar collagen gene, Col11a1, is essential for skeletal morphogenesis. *Cell* 80:423–430.
38. Kaplan FS, et al. (2008) Skeletal metamorphosis in fibrodysplasia ossificans progressiva (FOP). *J Bone Miner Metab* 26:521–530.
39. Feldman GJ, et al. (2007) Over-expression of BMP4 and BMP5 in a child with axial skeletal malformations and heterotopic ossification: a new syndrome. *Am J Med Genet A* 143:699–706.
40. Fukuda T, et al. (2009) Constitutively activated ALK2 and increased SMAD1/5 cooperatively induce bone morphogenetic protein signaling in fibrodysplasia ossificans progressiva. *J Biol Chem* 284:7149–7156.
41. Sakamoto A, Chen M, Kobayashi T, Kronenberg HM, Weinstein LS (2005) Chondrocyte-specific knockout of the G protein G(s)alpha leads to epiphyseal and growth plate abnormalities and ectopic chondrocyte formation. *J Bone Miner Res* 20:663–671.
42. Deirmengian GK, et al. (2008) Proximal tibial osteochondromas in patients with fibrodysplasia ossificans progressiva. *J Bone Joint Surg Am* 90:366–374.
43. Lounev VY, et al. (2009) Identification of progenitor cells that contribute to heterotopic skeletogenesis. *J Bone Joint Surg Am* 91:652–663.
44. Almeida MQ, et al. (January 27, 2010) Mouse Prkar1a haploinsufficiency leads to an increase in tumors in the Trp53+/– or Rb1+/– backgrounds and chemically induced skin papillomas by dysregulation of the cell cycle and Wnt signaling. *Hum Mol Genet*, 10.1093/hmg/ddq014.
45. Iliopoulos D, Bimpaki EI, Nesterova M, Stratakis CA (2009) MicroRNA signature of primary pigmented nodular adrenocortical disease: clinical correlations and regulation of Wnt signaling. *Cancer Res* 69:3278–3282.
46. Nadella KS, et al. (2008) Targeted deletion of Prkar1a reveals a role for protein kinase A in mesenchymal-to-epithelial transition. *Cancer Res* 68:2671–2677.
47. Siddappa R, et al. (2008) cAMP/PKA pathway activation in human mesenchymal stem cells in vitro results in robust bone formation in vivo. *Proc Natl Acad Sci USA* 105:7281–7286.
48. Jukes JM, et al. (2008) Endochondral bone tissue engineering using embryonic stem cells. *Proc Natl Acad Sci USA* 105:6840–6845.
49. Dahir GA, et al. (2000) Pluripotential mesenchymal cells repopulate bone marrow and retain osteogenic properties. *Clin Orthop Relat Res* (379, Suppl):S134–S145.
50. Siddappa R, et al. (December 23, 2009) Timing, rather than the concentration of cyclic AMP, correlates to osteogenic differentiation of human mesenchymal stem cells. *J Tissue Eng Regen Med*, 10.1002/term.246.
51. Siddappa R, et al. (2009) cAMP/PKA signaling inhibits osteogenic differentiation and bone formation in rodent models. *Tissue Eng Part A* 15:2135–2143.
52. Røsland GV, et al. (2009) Long-term cultures of bone marrow-derived human mesenchymal stem cells frequently undergo spontaneous malignant transformation. *Cancer Res* 69:5331–5339.
53. Skålhegg BS, et al. (2002) Mutation of the Calpha subunit of PKA leads to growth retardation and sperm dysfunction. *Mol Endocrinol* 16:630–639.
54. Rohlff C, Clair T, Cho-Chung YS (1993) 8-Cl-cAMP induces truncation and down-regulation of the RI alpha subunit and up-regulation of the RII beta subunit of cAMP-dependent protein kinase leading to type II holoenzyme-dependent growth inhibition and differentiation of HL-60 leukemia cells. *J Biol Chem* 268:5774–5782.
55. Pöch G (1971) Assay of phosphodiesterase with radioactively labeled cyclic 3′,5′-AMP as substrate. *Naunyn Schmiedebergs Arch Pharmakol* 268:272–299.
56. Nesterova M, Yokozaki H, McDuffie E, Cho-Chung YS (1996) Overexpression of RII beta regulatory subunit of protein kinase A in human colon carcinoma cell induces growth arrest and phenotypic changes that are abolished by site-directed mutation of RII beta. *Eur J Biochem* 235:486–494.